nature materials

SUPPLEMENTARY INFORMATION

DOI: 10.1038/NMAT3176

H-atom Relay Reactions in Real Space

T. Kumagai, A. Shiotari, and H. Okuyama

Department of Chemistry, Graduate School of Science, Kyoto University, Kyoto 606-8502, Japan

S. Hatta and T. Aruga

Department of Chemistry, Graduate School of Science, Kyoto University, Kyoto 606-8502, Japan and JST CREST, Saitama 332-0012, Japan

I. Hamada

WPI-Advanced Institute for Materials Research, Tohoku University, Sendai 980-8577, Japan

T. Frederiksen

Donostia International Physics Center (DIPC), 20018 San Sebastián, Spain and Division of Nano and New Functional Materials, Graduate School of Science and Engineering, University of Toyama, Toyama, 930-855 Japan

H. Ueba

Division of Nano and New Functional Materials, Graduate School of Science and Engineering, University of Toyama, Toyama, 930-855 Japan

(Dated: June 10, 2011)

DOI: 10.1038/NMAT3176

I. CHARACTERIZATION OF OH AND ATOMIC OXYGEN

By applying V=2 V and I=20 nA to a water molecule (Fig. S1a), we induced dissociation of a water molecule (Fig. S1). The first product appears as a double depression along [001] (Fig. S1b), which was assigned to a hydroxyl (OH) group based on the inelastic electron tunneling spectroscopy with the STM (STM-IETS) [1] that shows a vibration peak at 58 and 41 mV assigned to the OH and OD bending mode, respectively [2]. The hydroxyl group was further dissociated by applying V=0.9 V and I=10 nA to yield a round depression (Fig. S1c and Fig. 1a). We confirmed that the product is atomic oxygen by independent exposure of the surface to molecular oxygen which is known to be dissociated at similar temperature [3].

II. ASSEMBLY OF H_2O-$(OH)_3$ AND H_2O-$(OH)_4$ CHAINS

The H_2O-$(OH)_3$ complex was constructed by moving a H_2O-OH complex (Fig. S2a, left) to an OH dimer (center) in such a way that they were arranged in a straight line along [001] (Fig. S2b). It is noted that the manipulation of an isolated hydroxyl group was not feasible but its complex with water (H_2O-OH) was able to be moved along the $[1\bar{1}0]$ direction [4]. Schematic illustration of the reaction process is shown in Fig. S2c.

The H_2O-$(OH)_4$ complex was constructed as follows: First, two oxygen atoms were pre-

pared with the interatomic distance of $2b_0$ along [001] (Fig. S3a, b_0=3.62 Å is the atomic distance along [001]). Then two water molecules were sequentially reacted with oxygen atoms in the same way as Fig. 1 (Figs. S3b and S3c). The reaction resulted in the formation of an $(OH)_4$ chain. Finally, another water molecule was attached to the end of the $(OH)_4$ chain, yielding a H_2O-$(OH)_4$ complex (Fig. S3d).

III. MODEL FOR VIBRATIONALLY ASSISTED H-ATOM RELAY REACTION

Following Refs. [5, 6] and references herein, we here describe a theory to reproduce the exprimental results shown in Fig. 4, i.e., how the vibrational excitations of an H_2O-OH-OH (D_2O-OD-OD) complex can induce the H-atom transfer reaction. The reaction yield $Y(V)$ per electron is given by

$$Y(V) = \frac{R(V)}{I(V)} \tag{S1}$$

where $R(V)$ is the reaction rate and $I(V)$ the electrical current through the adsorbate level at an applied voltage V. For reactions induced by single-electron processes it is possible to express the reaction rate in terms of the vibrational generation rate $\Gamma_{\rm iet}$ and a prefactor K determined by the elementary process to activate the reaction-coordinate (RC) mode, i.e.,

$$R(V) = K\,\Gamma_{\rm iet}(V). \tag{S2}$$

We consider a given vibrational mode to be characterized by a certain vibrational density of states $\rho_{\rm ph}(\omega)$ and define the vibrational generation rate in terms of a spectral representation:

$$\Gamma_{\rm iet}(V) = \int_0^\infty d\omega \rho_{\rm ph}(\omega)\Gamma_{\rm in}(\omega, V), \tag{S3}$$

where $\Gamma_{\rm in}(\omega, V)$ is the spectral generation rate corresponding to an excitation of energy $\hbar\omega$. At low temperatures $k_BT \ll \hbar\Omega$, and at tunneling conditions $\Gamma_t \ll \Gamma_s$, the spectral generation rate takes to the well-known form [6]

$$\Gamma_{\rm in}(\omega, V) \approx \gamma_{\rm eh}(\omega)\frac{\Gamma_t}{\Gamma_s}\frac{|eV| - \hbar\omega}{\hbar\omega}\theta(|eV|/\hbar\omega - 1), \tag{S4}$$

DOI: 10.1038/NMAT3176

where Γ_s and Γ_t are the tunneling couplings (wide-band limit) to substrate and tip sides, respectively. Here $\gamma_{\rm eh}(\omega) = 4\pi\omega\chi^2\rho_a(\varepsilon_F)^2$ is the electron-hole pair damping with χ being the electron-vibration coupling and $\rho_a(\varepsilon_F)$ the adsorbate density of states at the Fermi energy ε_F. $\theta(x)$ is the Heaviside step function. Next, writing the current $I(V) = \sigma_0 V$ in terms of the junction conductance σ_0, we combine Eqs. (S1)-(S4) to the following expression for the reaction yield

$$Y(V) = K_{\rm eff}\,\frac{1}{V}\int_0^{|eV|} d\omega\;\rho_{\rm ph}(\omega)(|eV| - \hbar\omega), \tag{S5}$$

where the effective prefactor is $K_{\rm eff} = \frac{\gamma_{eh}(\Omega)}{\hbar\Omega\sigma_0}\frac{\Gamma_t}{\Gamma_s}K$. Here we assume a Gaussian distribution for the phonon density of states around a characteristic value Ω, i.e.,

$$\rho_{\rm ph}(\Omega, \sigma_{\rm ph}; \omega) = \frac{1}{\sigma_{\rm ph}\sqrt{2\pi}}\exp\Big(-\frac{(\omega-\Omega)^2}{2\sigma_{\rm ph}^2}\Big). \tag{S6}$$

The motivation for a Gaussian distribution is to take into account all broadening effects in a single parameter $\sigma_{\rm ph}$, in particular the nature of the broad spectrum of the OH (OD) stretch mode in a single hydrogen bond, but also other effects such as temperature, intrinsic life-time broadening, and instrumental ones [7]. Finally, when several, distinct accepting modes are involved, the total reaction yield should be expressed as the sum over accepting mode contributions:

$$Y(V) = \frac{1}{V}\sum_i K_{\rm eff}^i\int_0^{|eV|} d\omega\;\rho_{\rm ph}(\Omega_i, \sigma_i; \omega)(|eV| - \hbar\omega), \tag{S7}$$

Equations (S6) and (S7) constitute the formulas for the modeling in Fig. 4a, which work well to reproduce the experimental data.

IV. FIRST-PRINCIPLES SIMULATIONS

A. STM images and reaction pathway with STATE

We first carried out DFT calculations with a plane-wave basis set and ultrasoft pesudopotential method [8] as implemented in the STATE [9] code. Perdew-Burke-Ernzerhof (PBE) [10] generalized gradient approximation (GGA) was used for the exchange-correlation

functional. Plane-wave cutoffs of 36 Ry and 400 Ry were used to expand wave functions and augmentation charge, respectively. The Cu(110) surface was modeled by a five-layer slab with a 4×3 periodicity, and a vacuum region of 12.89 Å was inserted between slabs. The slab was constructed using the lattice constant optimized by PBE-GGA ($a = 3.64$ Å). An H_2O-$(OH)_2$ complex was put on one side of the slab and spurious electrostatic interaction was eliminated by the effective screening medium method [11]. Adsorbate and topmost two Cu layers were allowed to relax until the forces were less than 0.05 eV/Å, and remaining Cu atoms are fixed at their respective bulk positions. Brillouine zone sampling was done using a 4×2 Monkhorst-Pack [12] k-point set and Fermi-surface was treated by the first-order Methfessel-Paxton [13] scheme with the smearing width of 0.05 eV. For the STM simulations, we used a dense 16×8 k-point set. Adsorbate and topmost two Cu layers were allowed to relax, and remaining Cu atoms are fixed at their respective positions. STM simulations were conducted within the Tersoff-Hamman theory [14]. In the STM simulations, the sample bias voltage was set to 25 mV, and images were obtained at the constant height of 7 Å from the topmost Cu plane.

To complement the nudged elastic band (NEB) results from VASP for the reaction barrier (Fig. 5) we also calculated the potential energy surface by fixing the H-atom coordinate along the transfer direction ([001] direction), while other degrees of freedom, including the H-atom coordinates perpendicular to the transfer reaction, were fully relaxed. As shown in Fig. S5 this approach for the reaction pathway agrees very well with the NEB results (Fig. 4).

B. Vibrational modes and reaction pathway with VASP

We also carried out DFT calculations with the projector augmented wave method (PAW) and planewave basis as implemented in the VASP code (version 4.6) [15] with a similar setup as for the STATE calculations. We used the PBE-GGA exchange-correlation functional [10], a 515 eV energy cutoff, and a 4×2 Monkhorst-Pack [12] k-mesh. The Fermi surface was treated by the first-order Methfessel-Paxton [13] scheme with the smearing width of 0.05 eV. The force tolerance for the structural optimizations was 0.02 eV/Å for the ground state configuration. The Cu(110) surface was modeled by a five-layer slab with a 4×3 periodicity (lattice constant $a = 3.64$ Å) and a vacuum region of ~ 10 Å between the slabs. The adsorbates and topmost two Cu layers were relaxed. Vibrational modes and harmonic

DOI: 10.1038/NMAT3176

frequencies, calculated using the VASP finite diffence scheme with displacements of 0.02 Å, are reported in Tab. S1 and Figs. S6-S9 for both H and D species in ground state (GS) and transition state (TS) configurations.

In order to estimate the reaction barrier we used the nudged elastic band (NEB) method [16] with 12 floating images between the initial and final configurations. After convergence of the 12 images, the transition state was determined by another NEB calculation with just one floating image between the two images closest to the top of the barrier. The one-dimensional potential landscape is reported in Fig. 4 along with the corresponding geometries as insets. The force tolerance for the NEB calculation was set to 0.05 eV/Å. The reported total energy differences were evaluated using the tetrahedron method with Blöchl corrections using a Γ-centered mesh of 16×8 k-points. The resulting barrier of 0.25 eV is in good agreement with the results from the STATE calculations (Fig. S5).

[1] B.C. Stipe, M.A. Rezaei, and W. Ho, Science **280**, 1732 (1998).

[2] T. Kumagai, M. Kaizu, H. Okuyama, S. Hatta, T. Aruga, I. Hamada, Y. Morikawa, Phys. Rev. B **79**, 035423 (2009).

[3] B.G. Briner, M. Doering, H.-P. Rust, and A.M. Bradshaw, Phys. Rev. Lett. **78**, 1516 (1997).

[4] T. Kumagai, M. Kaizu, S. Hatta, H. Okuyama, T. Aruga, I. Hamada, Y. Morikawa, Phys. Rev. B **81**, 045402 (2010).

[5] S. G. Tikhodeev and H. Ueba, Phys. Rev. B **70**, 125414 (2004).

[6] S. G. Tikhodeev and H. Ueba, Phys. Rev. Lett. **102**, 246101 (2009)

[7] K. Motobayashi, Y. Kim, H. Ueba, and M. Kawai, Phys. Rev. Lett. **105**, 076101 (2010).

[8] D. Vanderbilt, Phys. Rev. B **41**, 7892 (1990).

[9] Y. Morikawa, H. Ishii, and K. Seki, Phys. Rev. **69**, 041403(R) (2004).

[10] J. P. Perdew, K. Burke, and M. Ernzerhof, Phys. Rev. Lett. **77**, 3865 (1996).

[11] M. Otani and O. Sugino, Phys. Rev. B **73**, 115407 (2006); I. Hamada, M. Otani, O. Sugino, and Y. Morikawa, *ibid.* **80**, 165411 (2009).

[12] H. J. Monkhorst and J. D. Pack, Phys. Rev. B **13**, 5188 (1976).

[13] A. Methfessel and A. T. Paxton, Phys. Rev. B **40**, 3616 (1989).

[14] J. Tersoff and D. R. Hamann, Phys. Rev. Lett. **20**, 1998 (1983).

[15] G. Kresse and J. Hafner, Phys. Rev. B **47**, 558 (1993); G. Kresse and J. Furthmüller, Phys. Rev. B **54**, 11169 (1996); G. Kresse and D. Joubert, Phys. Rev. B **59**, 1758 (1999).

[16] G. Mills, H. Jónsson, and G. K. Schenter, Surf. Sci. **324**, 305 (1995).

DOI: 10.1038/NMAT3176

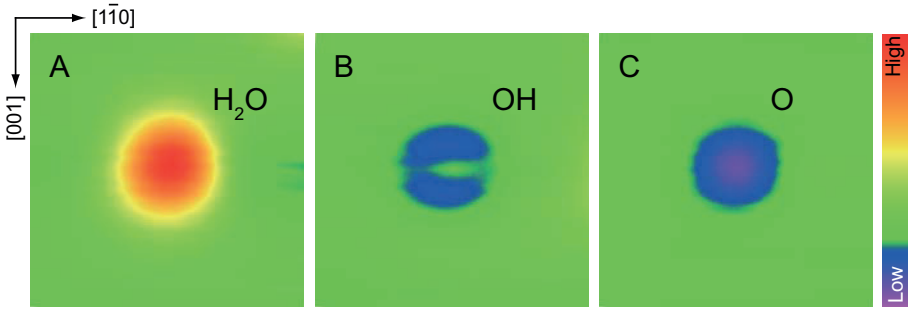

FIG. S1. STM images of (a) water molecule, (b) OH group, and (c) oxygen atom on Cu(110). The image size is 25×25 Å^2. The images were recorded (a) at V=14 mV and I=0.05 nA, and (b),(c) at V=24 mV and I=0.5 nA. The color bar corresponds to the topographic height from -0.20 Å(low) to 0.63 Å(high).

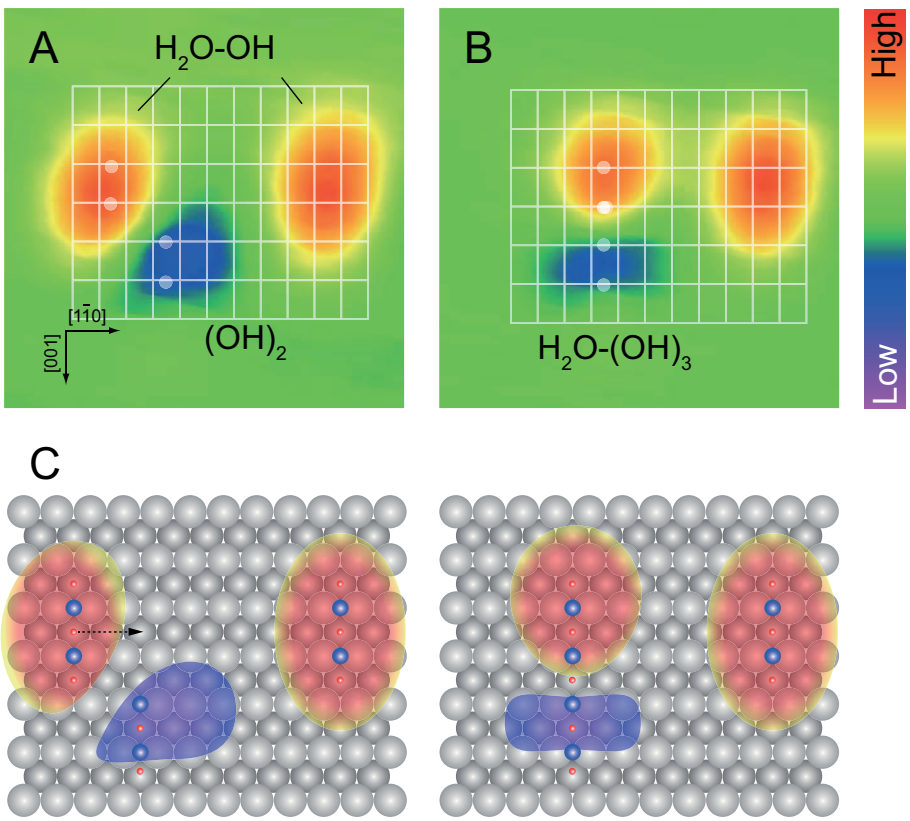

FIG. S2. (a),(b) Sequential STM images during the assembly process of the H_2O-$(OH)_3$ complex from $(OH)_2$ and H_2O-OH (38×38 Å^2, V=30 mV and I=0.5 nA). The white grid lines indicate the lattice of the Cu(110) surface and the dots represent the short-bridge sites occupied by oxygen atoms. The H_2O-OH complex was moved in the [1$\bar{1}$0] direction (dashed arrow) with STM, and reacted with $(OH)_2$ to yield a H_2O-$(OH)_3$ complex. (c) Schematic illustration of the reaction process. STM images of $(OH)_2$, H_2O-OH and produced chain complex are also depicted. The color bar corresponds to the topographic height from -0.35 Å(low) to 0.34 Å(high).

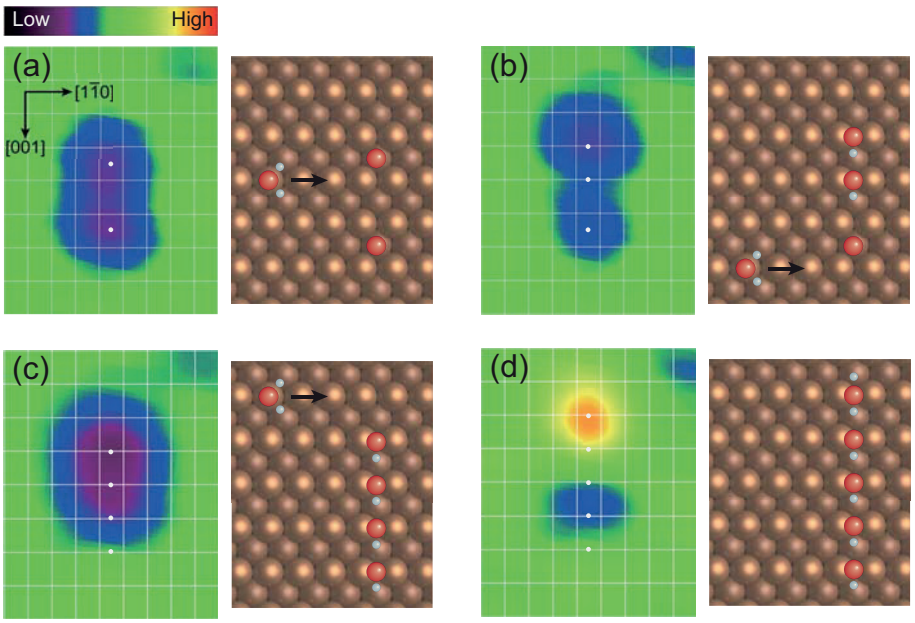

FIG. S3. Sequential STM images during the assembly process of the H_2O-$(OH)_4$ complex from two oxygen atoms and three water molecules, along with the schematic illustration of the reactions. (a) Two oxygen atoms were adsorbed along the [001] direction with the interatomic distance of $2b_0$. The two dots indicate the hollow sites on which oxygen atoms are adsorbed. (b) A water molecule was induced to react with an oxygen atom to yield $(OH)_2$+O. (c) A second water molecule reacted with another oxygen atom to yield $(OH)_4$. (d) Finally, a third water molecule was attaced to the end of $(OH)_4$, resulting in a H_2O-$(OH)_4$ chain complex. The dots in (c) and (d) indicate the the short-bridge sites occupied by oxygen atoms, although they are displaced from the exact short-bridge sites. The images were recorded at V=30 mV (23×29 Å^2). The tunnel current was I=0.2 nA for (a)-(c) and I=0.5 nA for (d). The color bar corresponds to the topographic height from -0.46 Å(low) to 0.35 Å(high).

DOI: 10.1038/NMAT3176

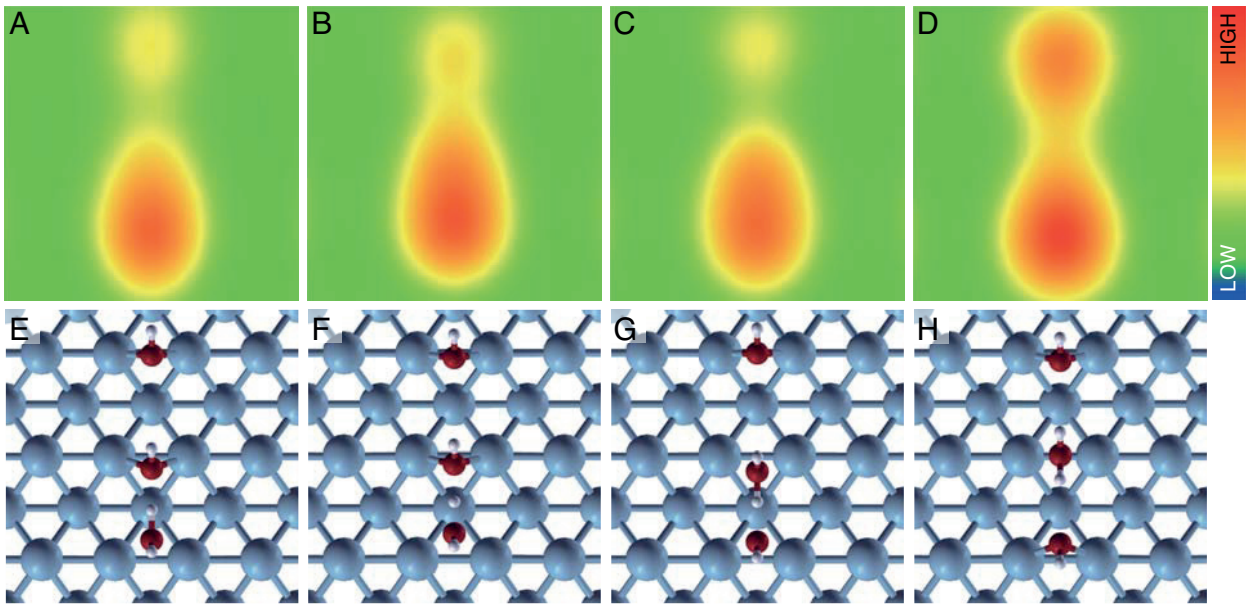

FIG. S4. Simulated STM images for (a) ground, (b) proton sharing, (c) intermediate state, and (d) transition states. Top views of corresponding structures are shown in (e)-(h), respectively.

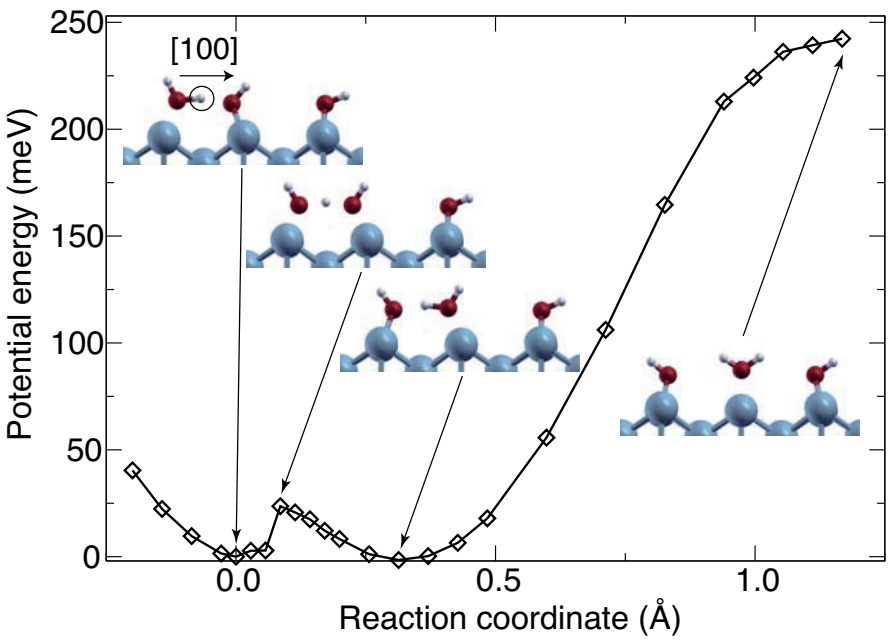

FIG. S5. Calculated potential energy for the H-atom transfer reaction in H_2O-$(OH)_2$/Cu(110) with the STATE code. The reaction coordinate is the distance of the transfered H atom (marked by a circle) along the [001] direction.

	GS_H	TS_H	GS_D	TS_D
Mode λ (index)	$\hbar\omega_\lambda$ (meV)	$\hbar\omega_\lambda$ (meV)	$\hbar\omega_\lambda$ (meV)	$\hbar\omega_\lambda$ (meV)
00	461.7	457.5	335.1	335.7
01	460.0	457.4	333.2	331.9
02	458.7	456.4	332.9	331.2
03	281.3*	439.5	206.0*	316.7
04	199.4	181.2	143.9	133.0
05	126.6	80.8	90.6	59.3
06	95.4	80.6	71.1	59.1
07	84.7	80.3	62.3	59.0
08	81.2	79.4	60.6	58.8
09	75.9	78.8	55.7	57.4
10	74.9	56.7	54.6	46.0
11	51.6	52.6	50.3	44.9
12	49.6	46.6	39.8	43.0
13	42.2	45.5	39.3	38.7
14	40.7	33.4	37.2	32.4
15	35.8	32.9	35.4	31.9
16	29.4	26.9	29.7	23.0
17	23.7	17.3	18.6	17.1
18	17.4	14.2	16.6	15.0
19	15.6	12.9	13.7	13.1
20	12.9	-15.5	12.5	-15.5
$\sum_{\omega>0}\hbar\omega_\lambda/2$	1359.3	1365.4	1019.5	1023.5

TABLE S1. Vibrational frequencies calculated within the harmonic approximation using VASP for the ground state (GS) and transistion state (TS) for both H and D species. Negative values indicate the imaginary mode frequency in the transition state. The zero-point energies (ZPE) (last row) indicate that the kinetic energy is slightly higher in TS than IS. The ZPE differences further suggest that the effective barrier is slightly higher for H than D species. The stretch modes OH* and OD* along the hydrogen bonds (marked with '*' in the table) are known to be highly anharmonic as well as strongly coupled to the slower intermonomer stretching modes that modulate the O–O distance. For comparison with experimentally observed frequencies these effects need to be considered. On a qualitative level the harmonic analysis highlights the spectacular softening of the stretch mode upon formation of a hydrogen bond.

DOI: 10.1038/NMAT3176

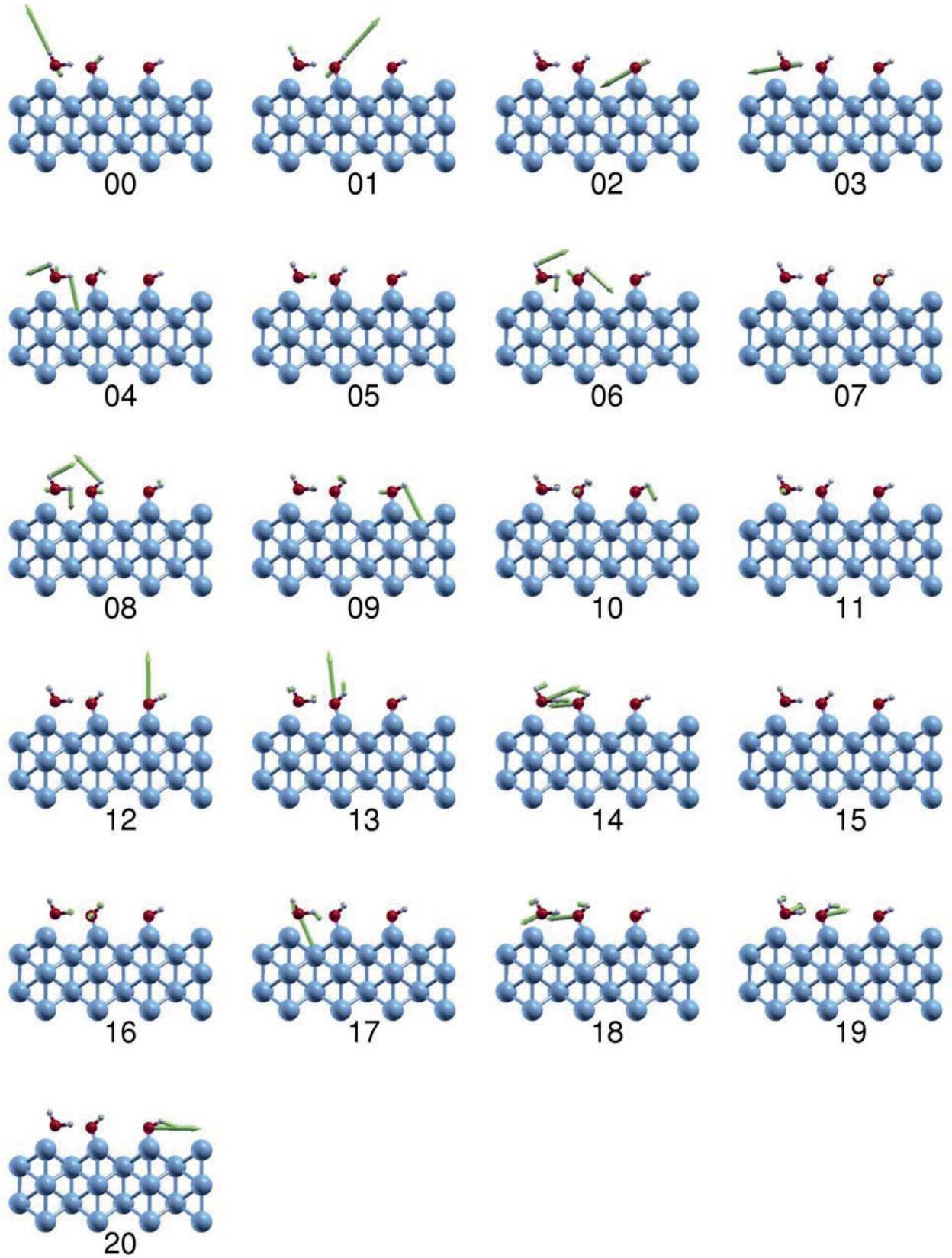

FIG. S6. Visualization of the normal modes for the ground state configuration (GS_H) of H_2O-$(OH)_2$. The mode labeling follows Tab. S1.

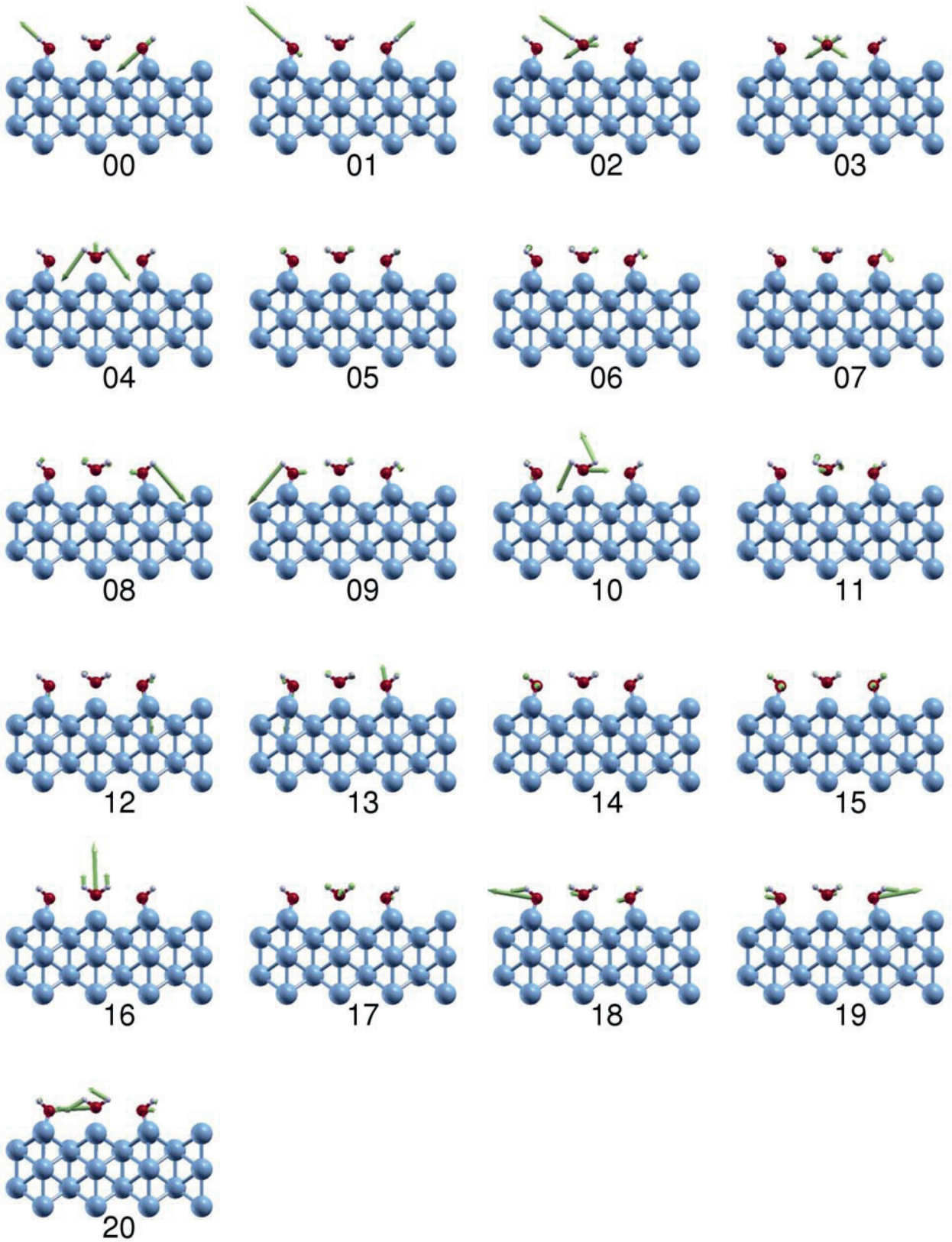

FIG. S7. Visualization of the normal modes for the transition state configuration (TS_H) of OH-H_2O-OH. The mode labeling follows Tab. S1.

DOI: 10.1038/NMAT3176

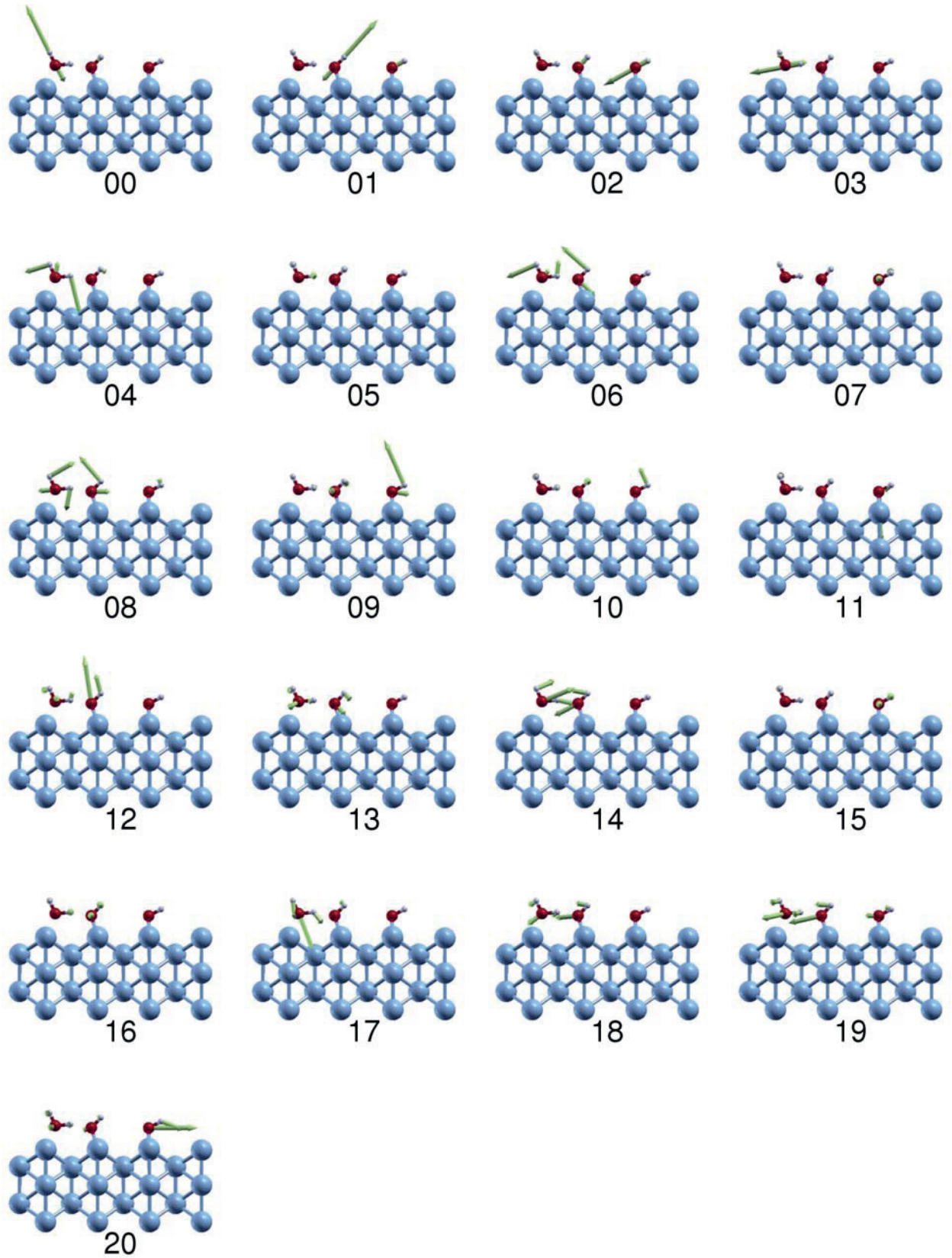

FIG. S8. Visualization of the normal modes for the ground state configuration (GS_D) of D_2O-$(OD)_2$. The mode labeling follows Tab. S1.

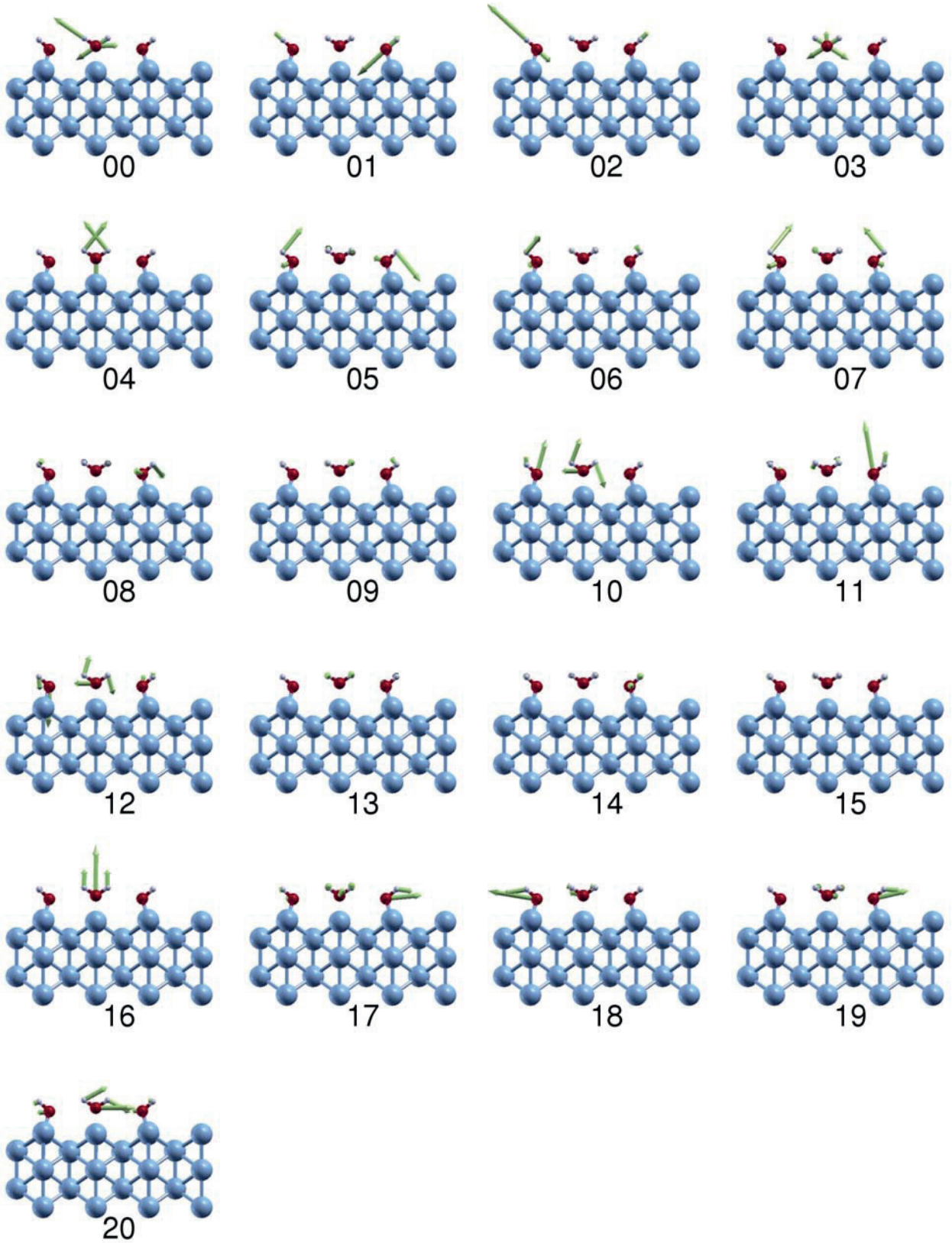

FIG. S9. Visualization of the normal modes for the transition state configuration (TS_D) of OD-D_2O-OD. The mode labeling follows Tab. S1.